PNAS

Supplementary Information for

The Influence of molecular design on structure-property relationships of a supramolecular polymer prodrug.

Kelsey G. DeFrates[1,†], Joakim Engström[1,2,†], Nivedina A. Sarma[2], Athiyya Umar[1], Jisoo Shin[1,2], Jing Cheng[1,2], Weiran Xie[3], Darrin Pochan[3], Ahmad K. Omar[2, 4], Phillip B. Messersmith[1,2,4*]

[1]Department of Bioengineering, University of California, Berkeley, Berkeley, CA 94720, USA.

[2]Department of Materials Science and Engineering, University of California, Berkeley, Berkeley, CA 94720, USA

[3]Department of Materials Science and Engineering, University of Delaware, Newark, DE 19716, USA

[4]Materials Sciences Division, Lawrence Berkeley National Laboratory, Berkeley, CA 94720, USA

[†] Contributed equally as first authors to this work.

* Correspondence: Phil Messersmith University of California, Berkeley, 210 Hearst Mining Building Berkeley, CA 94720-1760, USA

E-mail: philm@berkeley.edu; Tel.: 510-643-9631

This PDF file includes:

Supplementary Information Text

Materials. Poly(ethylene glycol) monomethyl ether was purchased from Sigma-Aldrich AB (CAS: 202495 9004-74-4) with M_n of 750 g/mol reported by the provider. Sodium bromide (NaBr) (≥99.0%, Sigma-Aldrich AB), sodium hypochlorite solution (NaClO) (Available chlorine 10-15 %, Sigma-Aldrich AB), 2,2,6,6-Tetramethyl-1-piperidinyloxy (TEMPO) (98%, Sigma-Aldrich AB) were used for PEG oxidation. 2-Amino-2-(hydroxymethyl)-1,3-propanediol (TRIS) (BioUltra, for molecular biology, ≥99.8% (T), Sigma-Aldrich AB CAS: 4109-02), 2-Amino-1,3-propanediol (serinol) (≥98%, Sigma-Aldrich AB CAS: 357898) or 2-Aminoethyl alcohol (ethanolamine) (≥98%, Sigma-Aldrich AB CAS: E9508) were coupled to PEG-structures using N,N,N′,N′-Tetramethyl-O-(1H-benzotriazol-1-yl)uronium hexafluorophosphate (HBTU) (≥99.0%, Sigma-Aldrich AB) and organic base N,N-Diisopropylethylamine (DIPEA) (ReagentPlus®, ≥99%, Sigma-Aldrich AB). DPCA was prepared as previously reported(1, 2) and activated using 1,1′-Carbonyldiimidazole (CDI) (reagent grade, Sigma-Aldrich AB). Reactions and precipitations were prepared using the following organic solvents, used as received: N,N-Dimethylformamide (DMF) (anhydrous, 99.8%, Sigma-Aldrich AB), Dichloromethane (DCM) (puriss. p.a., ACS reagent, reag. ISO, ≥99.9% (GC), Sigma-Aldrich AB), Diethyl ether (anhydrous, ACS reagent, ≥99.0%, contains BHT as inhibitor, Sigma-Aldrich AB), tetrahydrofuran (THF) (inhibitor-free, for HPLC, ≥99.9%, Sigma-Aldrich AB), Ethyl Alcohol, 200 Proof (EtOH) (Supelco via Sigma-Aldrich AB). Unless otherwise noted, any water used in this study was ultrapure (Milli-Q water) at < 0.05 µS cm-1. Sodium chloride (NaCl) (BioXtra, ≥99.5% (AT), Sigma-Aldrich AB), Sodium sulfate (Na2SO4, anhydrous for analysis EMSURE® ACS,ISO,Reag. Ph Eur, sodium hydroxide (NaOH, BioXtra, ≥98%, Sigma-Aldrich AB), sodium hydride (NaH, 60 % dispersion in mineral oil, Sigma-Aldrich AB), hydrochloric acid (HCl, 36.5-38.0%, BioReagent, for molecular biology solutions, Sigma-Aldrich AB) and Acetic acid (glacial 100%) (Suprapur®, Sigma-Aldrich AB) were all used as received.

Synthesis of DPCA and Im-DPCA. DPCA and activated Im-DPCA were prepared as previously reported (1, 2). Briefly, 8-aminoquinoline (14.4 g, 100 mmol) and diethyl ethoxymethylenemalonate (22.7 g, 105 mmol) were heated to 100℃ for 2 h and added to diphenylether (300 mL). The mixture was refluxed at 250℃ for 5 h, and then cooled to room temperature. The precipitate product was then separated by centrifugation, washed with hexane, and washed with diethyl ether. The resulting product was then combined with 10% (w/v) KOH or NaOH and heated for 2 hours at 100°C to obtain DPCA. DPCA was isolated following precipitation in dilute HCl, washed with deionized water, and dried under vacuum. For PEG coupling, DPCA (8 g, 33 mmol) was activated with 1,1'-carbonyldiimidazole (16 g, 100 mmol) in 150 mL DMF at 100°C for 3 hours to yield Im-DPCA. The product was separated by centrifugation and washed with diethyl ether, then dried under vacuum overnight. NMR-analysis in Figure S1. **^{1}H-NMR; 1,4-DPCA:** 9.2 ppm (1H) ((s), -C=N-C**H**=CH-C), 8.8 (1H) ((s), -C-NH-C**H**=C-C), 8.7 ppm (1H) ((d), -CH=C**H**-CH-), 7.9-8.4 ppm (3H) (residual aromatic protons), Figure SXa. **Im-DPCA:** 9.15 ppm (1H) ((s), -C=N-C**H**=CH-C), 8.5 ppm (1H) ((s), -C-NH-C**H**=C-C), 8.6 ppm (1H) ((d), -CH=C**H**-CH-), 7.8-8.3 ppm (3H) (residual aromatic protons), 8.22 ppm (1H) (Imidazole group), 7.7 ppm (1H) and 7.1 (1H) (Imidazole group), Figure S1.

Synthesis of PEG-OH$_1$, PEG-(OH)$_2$, and PEG-(OH)$_3$. Synthesis was inspired by previously published protocols, and adjusted to accommodate bivalent and monovalent linkers (2)**.** To generate PEG-COOH for further coupling, crude PEG-OH (10 mmol, 7.5 gram) was dissolved in ultrapure water (400 mL) with TEMPO (0.5 g, 3 mmol) and NaBr (0.5 g, 5 mmol) for 2h with stirring. The oxidation was then initiated by the addition of NaClO (10-15%, 40 mL, 90 mmol) to the PEG-solution while stirring. The pH of the reaction mixture was adjusted to 10 using NaOH (30wt% solution) and maintained throughout the reaction. After 45 minutes ethanol (20 mL) was added to quench the reaction and the pH was adjusted to 2.0 with HCl (10 vol%). The aqueous solution was then extracted with DCM (100 mL) four times, washed with brine, and dried with Na_2SO_4 and vacuum to yield PEG-COOH (25-30% yield). PEG-COOH (2 mmol, 1.53g) was then dissolved in 10 mL of DMF at 37°C. 2-Amino-2-(hydroxymethyl)-1,3-propanediol (4 mmol), 2-Amino-1,3-propanediol (4 mmol), or ethanolamine (4mmol) and DIPEA (4 mmol, 517 mg) were added to the DMF solution, followed by HBTU (3 mmol, 1.138 grams). The reaction was stirred at 37°C for 12 hours. Product was isolated by precipitation in diethyl ether at -20°C, redissolved in 100 mL DCM and purified through successive extractions with HCl (10 vol%, 10 mL), and washed with brine. The organic phase was dried

using Na_2SO_4, concentrated under vacuum, and precipitated in diethyl ether at -20°C overnight. The product was then redissolved in MeOH (10 mL), filtered using a 0.22 um syringe filter, precipitated in diethyl ether, isolated via centrifugation, and dried under vacuum (yield > 30wt%).

^{1}H-NMR; mPEG-OH: 3.25 ppm (3H) (-C**H3**, chain-end methyl group), 3.51 ppm (68H) (-C**H2**-C**H2**-O-, back bone PEG), 4.6 ppm (-OH, chain-end hydroxyl), Figure SXa. **mPEG-COOH:** 3.25 ppm (3H) (-C**H3**, chain-end methyl group), 3.51 ppm (68H) (-C**H2**-C**H2**-O-, back bone PEG), 4.0 ppm (2H) (-C**H2**-COOH, chain-end carboxyl), Figure SXb. **mPEG-1OH:** 3.25 ppm (3H) (-C**H3**, chain-end methyl group), 3.51 ppm (72H) (-C**H2**-C**H2**-O-, back bone PEG), 3.88 ppm (2H) (-C**H2**-COO-NH-, amide bond), 7.60 ppm (1H) (-OC-N**H**-CH2-, amide bond), 4.70 ppm (1H) (-CH2-CH2-O**H**, chain-end hydroxyl), Figure S2A. **mPEG-2OH:** 3.25 ppm (3H) (-C**H3**, chain-end methyl group), 3.51 ppm (72H) (-C**H2**-C**H2**-O-, back bone PEG), 3.90 ppm (2H) (-C**H2**-COO-NH-, amide bond), 7.20 ppm (1H) (-OC-N**H**-CH-, amide bond), 4.69 ppm (2H) (-CH-(CH2-O**H**)$_2$, chain-end hydroxyls), Figure S2B. **mPEG-3OH:** 3.25 ppm (3H) (-C**H3**, chain-end methyl group), 3.51 ppm (72H) (-C**H2**-C**H2**-O-, back bone PEG), 3.88 ppm (2H) (-C**H2**-COO-NH-, amide bond), 7.02 ppm (1H) (-OC-N**H**-CH-, amide bond), 4.80 ppm (3H) (-C-(CH2-O**H**)$_3$, chain-end hydroxyls), Figure S2C. DPCA-region detailed in Figure SX. **MALDI-TOF-MS** [m/z] main mass peak; **mPEG-OH**: 760 g/mol, **mPEG-COOH:** 818 g/mol, **mPEG-1OH:** 905 g/mol, **mPEG-2OH:** 935 g/mol, **mPEG-3OH:** 965 g/mol, Figure S3.

Coupling of DPCA for P7D1, P7D2, and P7D3. mPEG-(OH)$_x$ was coupled to DPCA using CDI-activated esterification, as previously described (2). Minor adjustments were made to the previously published protocol to include mPEG-OH and mPEG-(OH)$_2$. Briefly, mPEG-(OH)$_x$ (1 mmol) was dissolved in 5 mL DMF at 50°C and dried under vacuum. NaH (60% in oil, 2 molar eq to -OH) was then added while stirring. After 10 minutes, the Im-DPCA compound was added and left to react at 50 °C for 30 minutes. A dark brown, highly viscous solution was then obtained. The crude solution was precipitated in diethyl ether at 1:10 volume ratio and kept for 1 hours at -20°C, before centrifugation at -10°C for 5 minutes at 5000 rpm. The supernatant was discarded, and the pellet dried under vacuum for 2 hours. To separate free DPCA, the dried pellet was redissolved in methanol at 50 mg/mL and filtered through a 0.45 um filter into diethyl ether at -20°C. The final product, consisting of PEG-DPCA and potentially free uncoupled DPCA and PEG, is then subjected to further purification via HPLC or column chromatography. ^{1}H-NMR spectra are shown in Figure S4.

PEG-DPCA Reaction Scheme

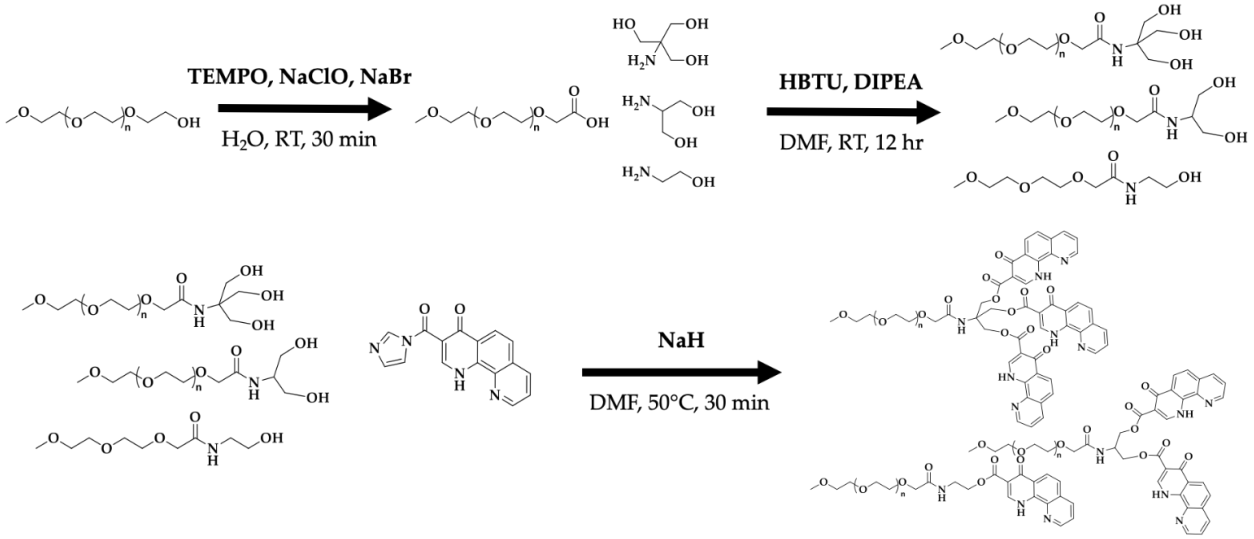

^{1}H-NMR; P7D1: 3.25 ppm (3H) (-C**H3**, chain-end methyl group), 3.51 ppm (70H) (-C**H2**-C**H2**-O-, back bone PEG), 3.94 ppm (2H) (-C**H2**-COO-NH-, amide bond), 4.27 ppm (2H) ((d), ((-CH2-C**H2**-DPCA), 7.90 ppm (1H) (-OC-N**H**-CH-, amide bond), 9.10 ppm (1H) ((s), -C=N-C**H**=CH-C, in coupled DPCA region), 8.7 ppm

(1H) ((d), -CH=C**H**-CH-, in coupled DPCA region), 7.8-8.0 ppm (3H) (residual aromatic protons on DPCA coupled), 12.9 ppm (1H) (amide proton in DPCA), Figure S4. **P7D2:** 3.25 ppm (3H) (-C**H3**, chain-end methyl group), 3.51 ppm (70H) (-C**H2**-C**H2**-O-, back bone PEG), 3.94 ppm (2H) (-C**H2**-COO-NH-, amide bond), 4.4 ppm (4H) ((d), (-CH-(C**H2**-DPCA)$_2$, 7.90 ppm (1H) (-OC-N**H**-CH-, amide bond), 9.10 ppm (1H) ((s), -C=N-C**H**=CH-C, in coupled DPCA region), 8.7 ppm (1H) ((d), -CH=C**H**-CH-, in coupled DPCA region), 7.8-8.0 ppm (3H) (residual aromatic protons on DPCA coupled), 12.9 ppm (1H) (amide proton in DPCA), **P7D3:** 3.25 ppm (3H) (-C**H3**, chain-end methyl group), 3.51 ppm (70H) (-C**H2**-C**H2**-O-, back bone PEG), 3.94 ppm (2H) (-C**H2**-COO-NH-, amide bond), 4.7 ppm (6H) ((d), (-C-(C**H2**-DPCA)$_3$, 7.90 ppm (1H) (-OC-N**H**-CH-, amide bond), 9.10 ppm (1H) ((s), -C=N-C**H**=CH-C, in coupled DPCA region), 8.7 ppm (1H) ((d), -CH=C**H**-CH-, in coupled DPCA region), 7.8-8.0 ppm (3H) (residual aromatic protons on DPCA coupled), 12.9 ppm (1H) (amide proton in DPCA), **MALDI-TOF-MS** [m/z] main mass peak; **P7D1**: 1125 g/mol, **P7D2:** 1463 g/mol, **P7D3:** 1628 g/mol.

Nuclear magnetic resonance (NMR). Chain-end modification and purity of mPEG-OHs and DPCA coupling reactions was monitored using solution state ^{1}H-NMR. Spectra were obtained in DMSO-d6 using a Bruker Avance 400 console with Oxford Instruments 9.4 T magnet (AVB-400 MHz) NMR, Bruker Avance III 600 console with Bruker 14 T magnet (AV-600 MHz) NMR or Bruker Avance-III 300 MHz NMR instrument.

Matrix-assisted lased-deposition ionization Time-of-flight mass spectrometry (MALDI-TOF-MS). Final PEG-DPCA structures as well as intermediates (PEG-OH, PEG-COOH, PEG-(OH)$_x$) /PEG-2OH/PEG- were analyzed with MALDI-ToF-MS using a Applied Biosystems Voyager DE Pro (QB3/Chemistry Mass Spectrometry Facility at UC Berkeley). All samples were prepared in ACN/water mixtures and sandwiched between layers of α-Cyano-4-hydroxycinnamic acid (CHCA) (Sigma-Aldrich AB) matrix, prepared from an ethanol solution.

Purification of PEG-DPCAs using Semi-Preparative HPLC. After synthesis, dried PEG-DPCAs were dissolved in 70/30 H_2O/ACN solutions, filtered using a 0.22 um syringe filter, and manually injected into an Agilent 1260 Infinity Series HPLC in semi-preparative mode, equipped with a Zorbax SB-C18 column (5 µm, 9.4x250 mm, 80Å pores, silica; 10%). Fractions of DPCA, partially coupled conjugates, and pure PEG-DPCAs, were then separated using a 70/30 to 0/100 H_2O/ACN mobile phase gradient ramped over 30 minutes at 4 ml/min. UV-vis signal at DPCA λ_{max}, of 261 nm and 316 nm was followed.

Purification of PEG-DPCAs using column chromatography. After synthesis, dried PEG-DPCAs were dissolved in 50/50 H_2O/ACN solution at 10 g/L. 100 mL of the PEG-DPCA solution was loaded into a packed column of Silica Gel (grade 60 Mesh 230-400) in 50/50 H_2O/ACN with a bottom layer of sand. Fractions of DPCA and pure PEG-DPCAs, were then separated using a 50/50 H_2O/ACN mobile phase with constant flow rate 1.25 mL/min for 120 minutes. DPCA fractions were gathered after 35 minutes and PEG-DPCA pure fractions eluted after 80 minutes, as confirmed by analytical HPLC, NMR, and MALDI-TOF-MS. Fractions were also analyzed through thin-layer chromatography using a UV-lamp to detect DPCA.

Analysis of PEG-DPCAs using Analytical HPLC. The purity of PEG-DPCA conjugates and quantity of free DPCA in hydrolysis, release, and enzymatic cleavage studies was assessed using an Agilent 1260 Infinity Series HPLC equipped with a UV-Vis detector and Zorbax C18 column (10 µm, 4.6x250 mm, 300Å pores, silica; 2-100%). A 70/30 to 0/100 H_2O/ACN with 0.1% TFA gradient ramped over 30 minutes was used as the mobile phase. UV-vis signal at DPCA λ_{max}, of 261 nm and 316 nm was followed and peak integrals from the chromatogram were converted to concentration using standard curves prepared from solutions of known drug content.

TEM. Aqueous suspensions of self-assembled PEG-DPCA conjugates prepared at 7g/L were drop-casted onto carbon-coated copper grids (Electron Microscopy Sciences, CF400-Cu). After 5 minutes, excess liquid was removed by blotting with filter paper. For stained samples, a 1% uranyl acetate aqueous solution was added to the grid for 3 minute and blotted with filter paper. TEM images were taken on a FEI Tecnai 12 transmission electron microscope (Electron Microscopy Lab, UC Berkeley).

DLS Measurements. The hydrodynamic radius (D_H) and polydispersity index (PDI) of the self-assembled PEG-DPCAs was determined with a Malvern Zetasizer NanoZS at 25 °C at concentrations of 7 mg/mL in H_2O. For DLS measurements, warmed solutions were filtered through a 0.22 μM syringe filter prior to cooling. Due to the presence of non-spherical aggregates in P7D2 and P7D3, DLS is not reported for these samples.

SAXS measurements: Transmission SAXS analysis was performed on beamline 7.3.3 of the Advanced Light Source (Lawrence Berkeley National Laboratory, Berkeley, USA) using a 10 keV synchrotron X-ray beam with a Mo/B4C double-multilayer monochromator and a detector distance of 3.535 m, providing a feasible q-range of ~0.004−0.3 Å-1 (the beam size was 200 μm × 200 μm and the detector a Pilatus 2M). Self-assembled PEG-DPCAs (P7D1, P7D2 and P7D3) were analyzed at 25 g/L in 1 mm quartz glass capillary tubes (wall thickness 0.01 mm) using an exposure time of 20 seconds. The 1D scattering profiles were obtained by radial integration of 2D patterns using the pyFAI package with the scattering of a water solution in the capillary subtracted as background (3).

Rheological measurements. The rheological properties of self-assembled PEG-DPCAs in PBS buffer and control samples were determined using an oscillatory rheometer (MCR-302 modular compact rheometer from Anton Paar) with a cone-plate geometry (25 mm diameter, 1°). At 25°C, viscosity and shear stress was monitored as shear rate was ramped logarithmically from 0.01 to 1000 s -1 in fixed measurement point duration mode, for 2s over 200s to collect 100 total points.

Ultraviolet–visible spectroscopy (UV-Vis). UV-Vis spectra of prodrugs and free DPCA were collected from 200 to 500 nm using a Shimadzu UV 2600 Spectrophotometer. All prodrug samples were prepared at 0.1 mg/mL in DI H_20 with heating and vortexing. Once cooled, 0.7 mL of sample were transferred to BrandTech Disposable UV-Cuvettes with 8.5 mm path length (product #759210). Cuvettes filled with DI H_20 were used as reference. For free drug samples, saturated solutions of DPCA were prepared by suspending DPCA in DI H_2O. After two days of incubation at room temperature, solutions were centrifuged and filtered to remove undissolved drug. Samples were then diluting with H_2O to determine possible concentration effects.

Differential scanning calorimetry (DSC): DSC analysis was performed on pure 1,4-DPCA with a Mettler Toledo DSC. DPCA was analyzed with a heating and cooling rate of 2 or 10 °C/min in nitrogen atmosphere. The method used was comprised of 2 heating cycles and 1 cooling; heating from 25 to a maximum of 350 °C, equilibrium for 5 min to clear out the history of the materials, then cooling down to -50 °C to attempt detection of crystallization, followed by a second heating to maximum 350°C. With no distinct peaks detected for neither cooling nor second heating, the data from the first heating was used to calculate the enthalpy of fusion for the molecule by measuring the energy needed to melt the crystals (ΔH_{fusion}). An average of the ΔH_{fusion} for three different heating cycles was used to calculate a value for comparison with modelling methods, including also attempts of lower end-temperature target.

Molecular Dynamics Simulations. The dynamics of our system correspond to the overdamped limit in which the inertia of the beads is negligible. As a result, the forces acting on the i^{th} bead identically sum to zero, and obey the following:

$$\boldsymbol{F}_i^B + \boldsymbol{F}_i^D + \boldsymbol{F}_i^P = \mathbf{0}, \qquad (S1)$$

where $\boldsymbol{F}_i^B$ and $\boldsymbol{F}_i^D$ represent the nonconservative stochastic and dissipative forces, respectively, exerted by the implicit solvent on each bead while $\boldsymbol{F}_i^P$ represents both bonded and non-bonded conservative interparticle forces. The beads are connected by a FENE potential using the canonical Kremer-Grest parameters(4) with a spring constant $k = 30k_BT/\sigma^2$ and maximal stretched bond length $r_0 = 1.5\sigma$.

Rigid Body Constraint. We fix the relative intramolecular positions of the DPCA beads by applying a rigid body constraint algorithm in HOOMD-blue (5). The rigid body is comprised of the DPCA beads and the

single connecting polymer bead. The remaining polymer beads are flexible and excluded from the rigid body. The rotational axis of the rigid body is chosen to be the coordinate center of the constituent particles. In each rigid body, the DPCA beads and the connecting polymer bead were separated by a distance of 0.85σ, which ensures that the rigid body strictly excludes other beads. The translational drag coefficient γ of the rigid body is set to be the single particle drag coefficient ζ multiplied by the number of beads within the rigid body (i.e., $= 2\zeta, 3\zeta,$ and 4ζ for P7D1, P7D2, and P7D3 respectively). We set the rotational drag to be $\gamma_R = 4\gamma\sigma_{\text{eff}}^2/3$ where σ_{eff} is the effective radius of the rigid body (following the convention of Nguyen et. al.(6)) computed from the coordinate positions of the constituent particles. The choice of γ_R, of course, does not affect equilibrium statistics.

Implicit Solvent Model. The fluctuating and dissipative forces imparted by the implicit solvent on our molecules are taken to have the following form in accordance with the fluctuation dissipation theorem:

$$\langle \boldsymbol{F}_i^B(t)\rangle = \mathbf{0}, \qquad \textit{(S2)}$$

$$\langle \boldsymbol{F}_i^B(t)\boldsymbol{F}_j^B(t')\rangle = 2k_BT\,\zeta\delta_{ij}\delta(t-t')\mathbf{I}, \qquad \textit{(S3)}$$

$$\boldsymbol{F}_i^D = -\zeta\boldsymbol{v}_i, \qquad \textit{(S4)}$$

where ζ is the drag coefficient, δ_{ij} is the Kronecker delta, $\delta(t-t')$ is the Dirac delta, $\mathbf{I}$ is the identity tensor, and $\boldsymbol{v}_i$ is the velocity of particle i. A basic unit of time arising from these dynamics is the single-bead diffusion time defined as $\tau = \sigma^2\zeta/k_BT$. We set our simulation timestep to be $5 \times 10^{-6}\tau$.

Molecular Dynamics Equilibration Procedure. All molecules were initially arranged in a cubic lattice. We conduct a relatively short (1000τ) initial simulation with $\varepsilon_A = 1k_BT$ in order to randomize the molecular configurations. Subsequently, the DPCA-DPCA attraction ε_A is set to the desired value and the simulation is run for a duration of $10^5\tau$. We subsequently analyze the clusters resulting from this trajectory to compute the characteristic relaxation time of the system. For these relatively dilute systems, the limiting step for cluster growth is for two separated clusters to diffuse to each other and merge. We therefore take the characteristic timescale of the system to be the average time for clusters to diffuse the average intercluster distance. This distance is given by $r = \rho^{-1/3}$, where ρ is the cluster number density. In the free-draining limit, the diffusivity of a cluster with M molecules will obey a Stokes-Einstein relation with a drag coefficient given by the total number of beads MN (N is the number of beads per molecule) in the cluster multiplied by the single bead drag coefficient ζ. The average diffusivity of a cluster is then simply related to the average cluster size $\langle M\rangle$ with $\langle D\rangle = k_BT/\langle M\rangle N\zeta$. The characteristic cluster aggregation time then given by $\tau_{\text{relax}} = r^2/\langle D\rangle$. Upon computing this relaxation time for simulations run at $\phi = 0.002, 0.005,$ and 008, we extended the simulation trajectory for at least $2\tau_{\text{relax}}$ to allow for cluster merging events.

Unit Conversion. The simulation volume fraction ϕ is the concentration of polymer-drug conjugate divided by its molecular density. The approximate density values for each PEG-DPCA system and the corresponding concentrations for the lower and upper bounds of ϕ are given below.

Table S1: Conversion between simulation volume fraction ϕ and experimental concentration (g/L)

P7Dn	Approximate density	ϕ = 0.0008	ϕ = 0.002	ϕ = 0.005	ϕ = 0.008
P7D1	1179.191 g/L	0.94 g/L	2.4 g/L	5.6 g/L	9.4 g/L
P7D2	1231.606107 g/L	0.99 g/L	2.5 g/L	6.2 g/L	9.9 g/L
P7D3	1255.527 g/L	1 g/L	2.5 g/L	6.3 g/L	10 g/L

The DPCA attraction strength ε_A was estimated from DSC measurements of pure DPCA. The variance in the enthalpy of fusion results in an estimated lower bound of $\Delta H_{fus} = 39$ kJ/mole (corresponding to $\varepsilon_A = 5.52k_BT$) and upper bound of $\Delta H_{fus} = 92$ kJ/mole ($\varepsilon_A = 13.02k_BT$). Figure S12 explores this range of

parameter ε_A and confirms that the trends observed in the main text for $\varepsilon_A = 12.5k_BT$ hold for all attraction strengths.

Quantifying cluster shape. We measured the asphericity b of each cluster to compute the asphericity probability density function $p(b)$ (see Figure S12). We observed that the average asphericity for self-assembled clusters of P7D3 is consistently larger than that of P7D1 and P7D2 at every attraction strength.

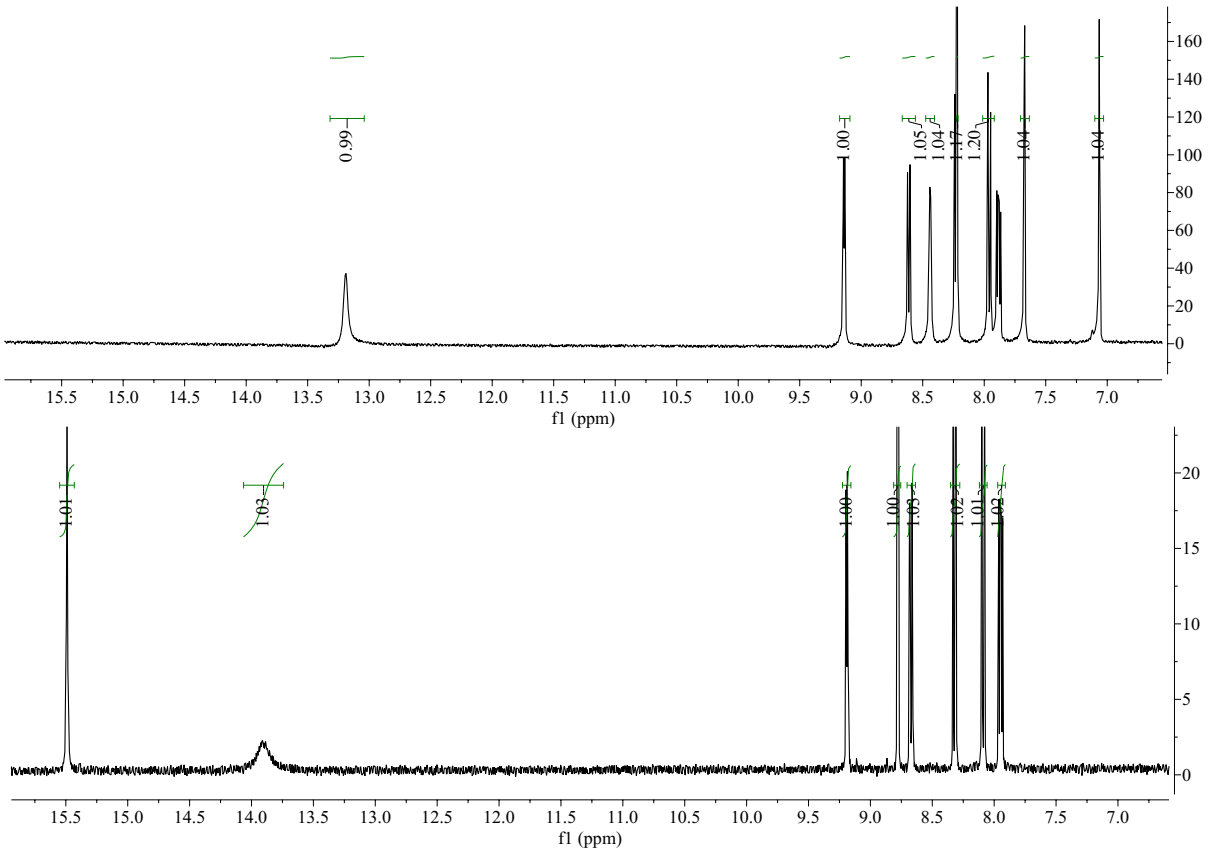

Fig. S1. [1]HNMR analysis of DPCA (bottom) and activated Im-DPCA (top) used in synthesis.

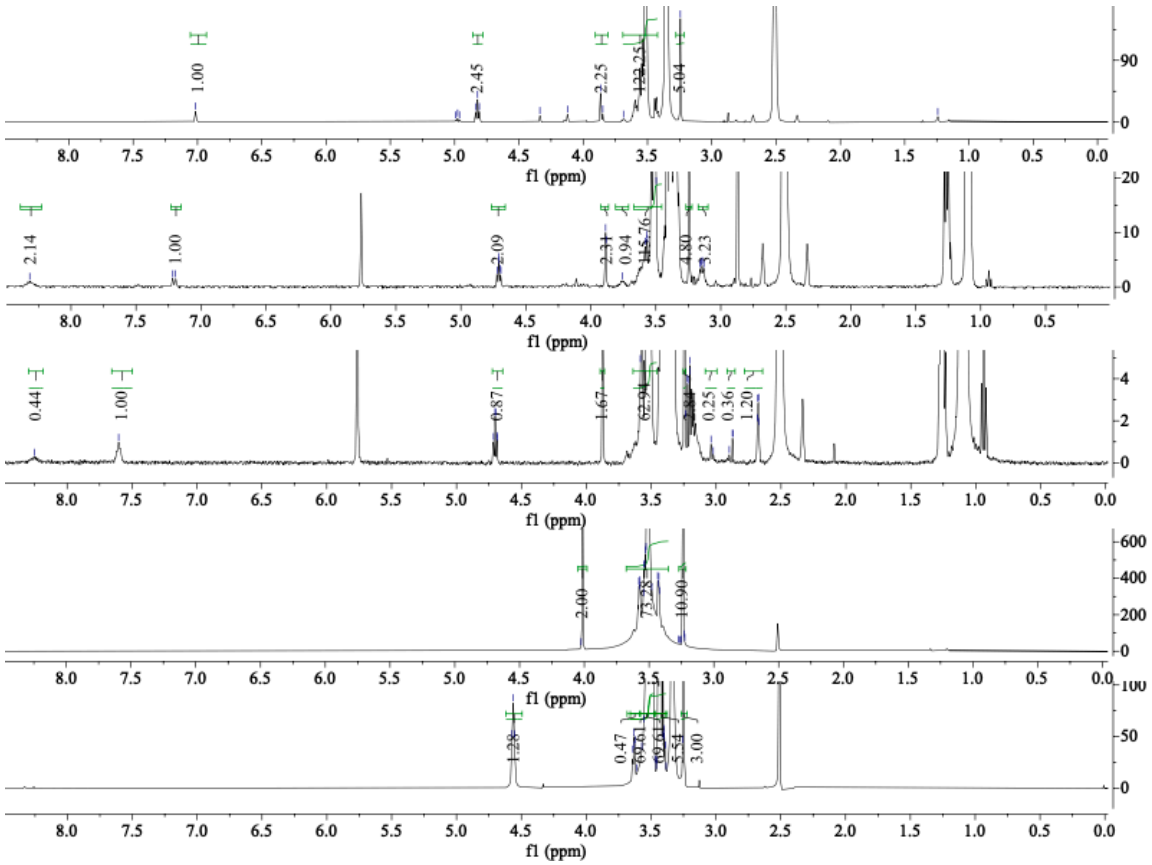

Fig. S2. ^{1}H-NMR of (bottom to top) unmodified PEG, oxidized PEG-COOH, PEG-OH, PEG-$(OH)_2$, and PEG-$(OH)_3$.

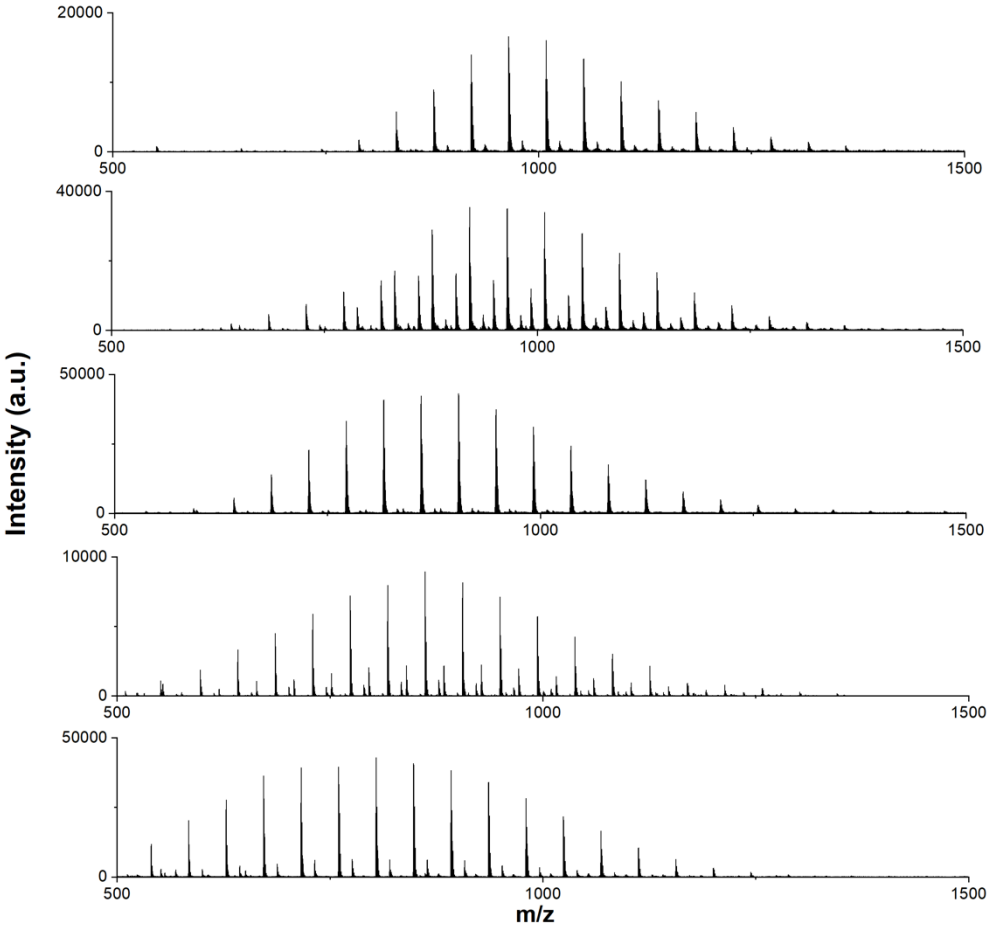

Fig. S3. MALDI-TOF-MS spectra of (from bottom to top) unmodified PEG, oxidized PEG-COOH, PEG-OH, PEG-$(OH)_2$, and PEG-$(OH)_3$.

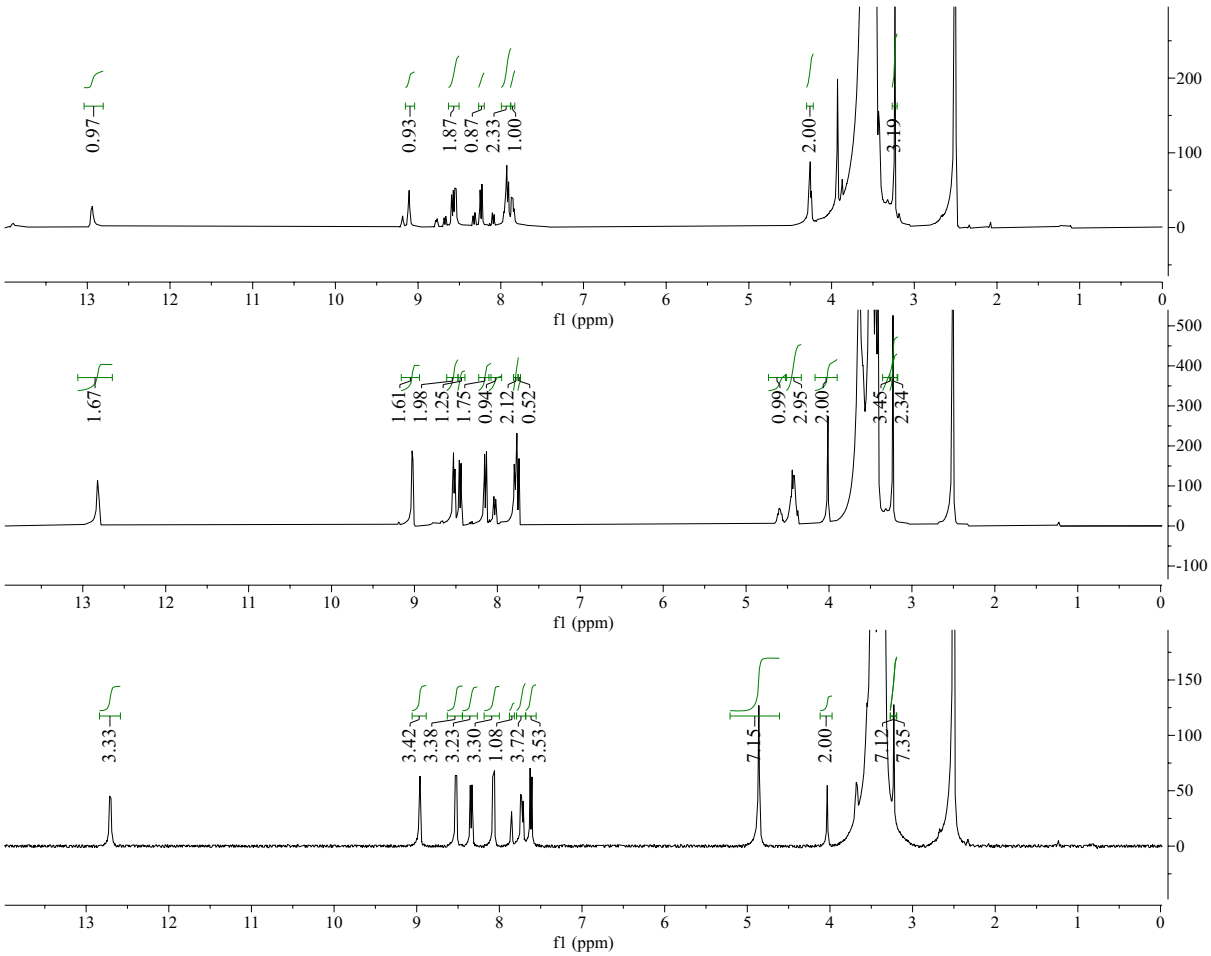

Fig. S4. [1]HNMR analysis of PEG-DPCA prodrugs, (from top to bottom) P7D1, P7D2, and P7D3.

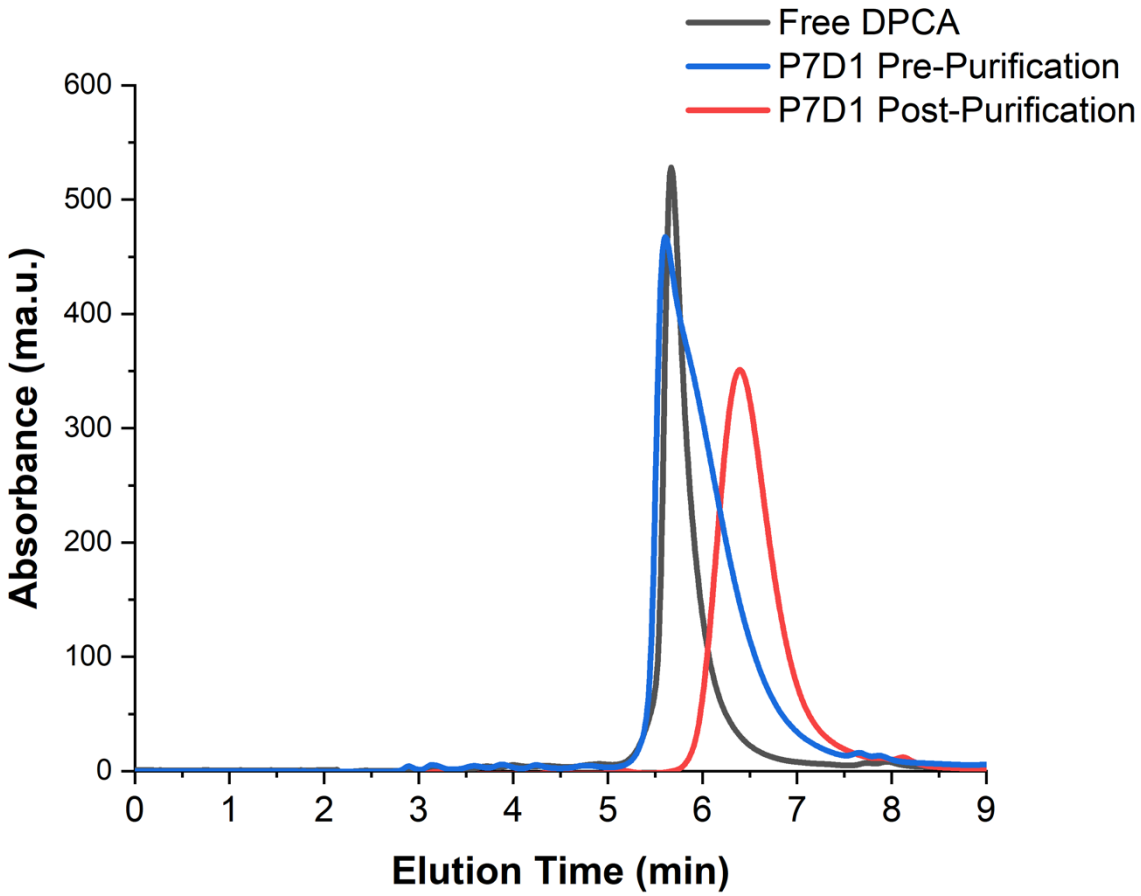

Fig. S5. Analytical HPLC chromatograms of example PEG-DPCA before (blue) and after (red) purification via silica gel column. Removal of free DPCA (black) is clearly shown.

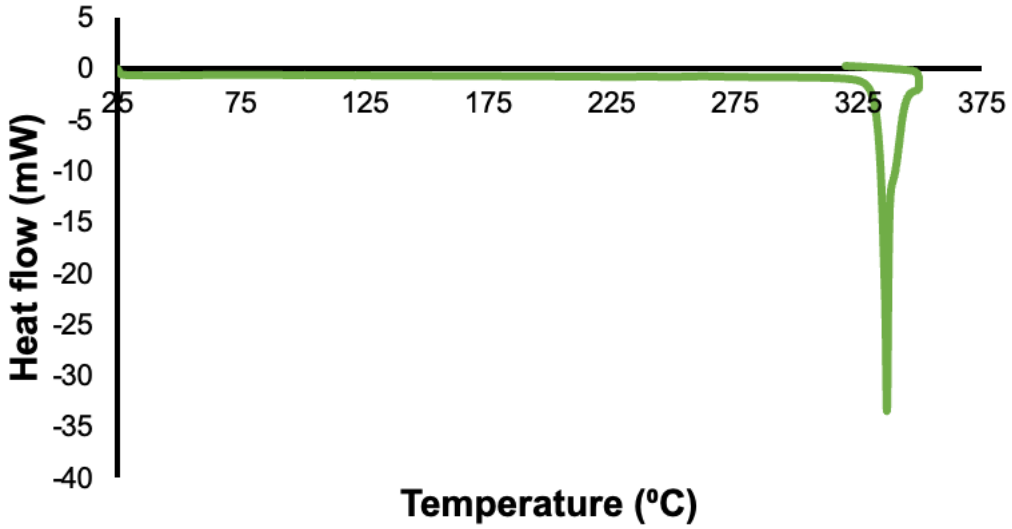

Fig. S6. Representative DSC analysis of DPCA during a 10ºC /min heating cycle between 25-350 ºC. No crystallization peak was visible during cooling.

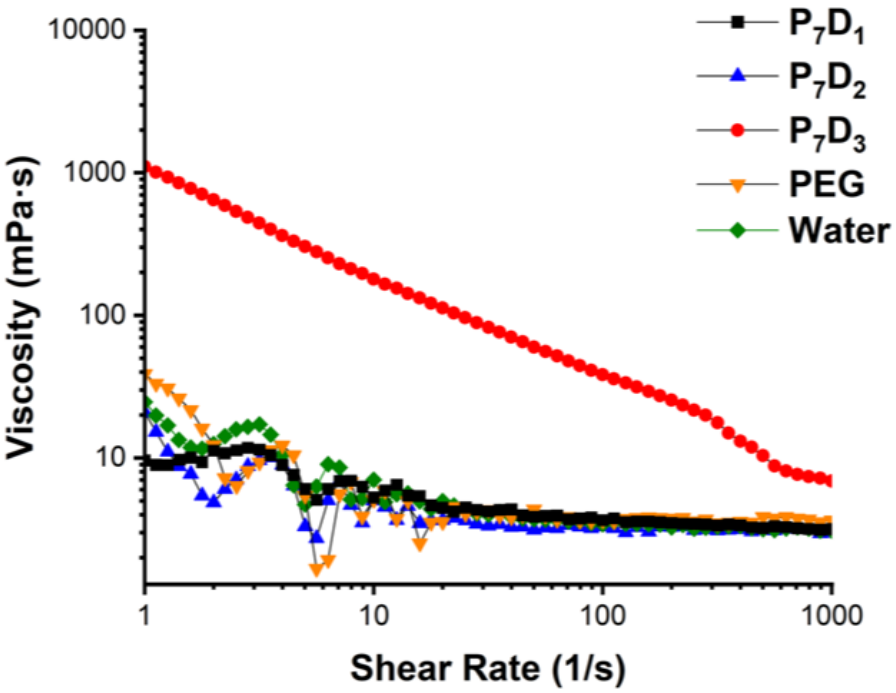

Fig. S7. Rheological behavior of PEG-DPCA prodrugs and reference samples in response to increasing shear rate.

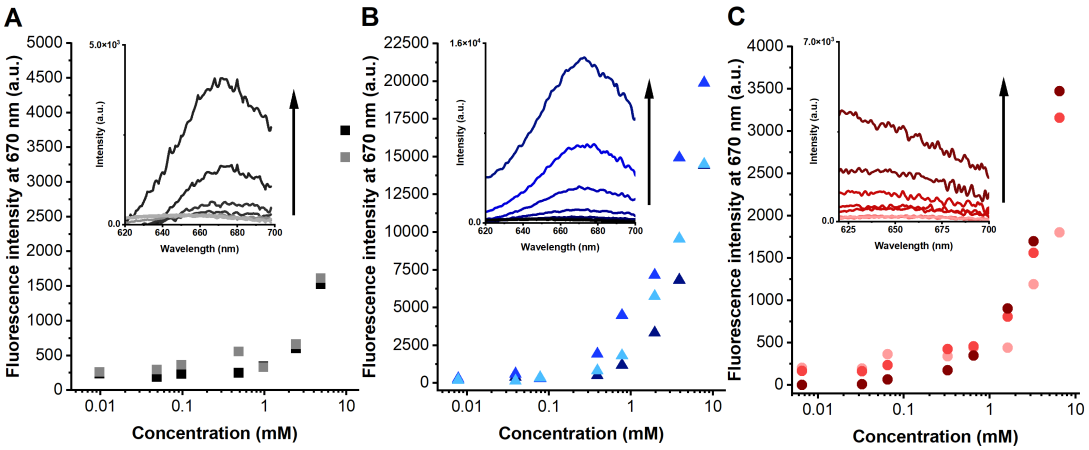

Fig. S8. Raw data showing dependence of Nile red fluorescence on P7D1 (A), P7D2 (B), or P7D3 (C) used to extract CMC values.

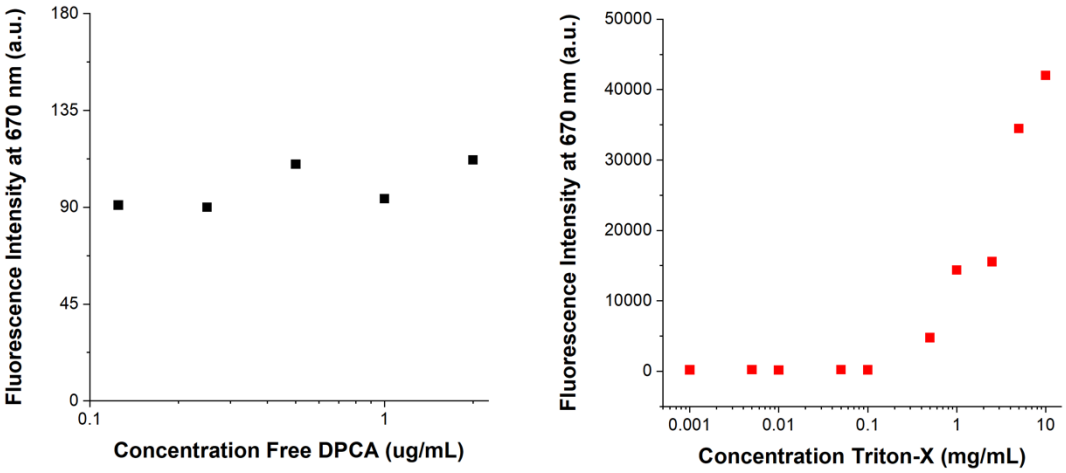

Fig. S9. Model CMC assay preformed with DPCA alone, showing no changes in probe emission with increasing drug concentration alone (A). Results of nile red probe CMC assay using Triton X. CMC of 0.4 mM is estimated, in good agreement with literature values.

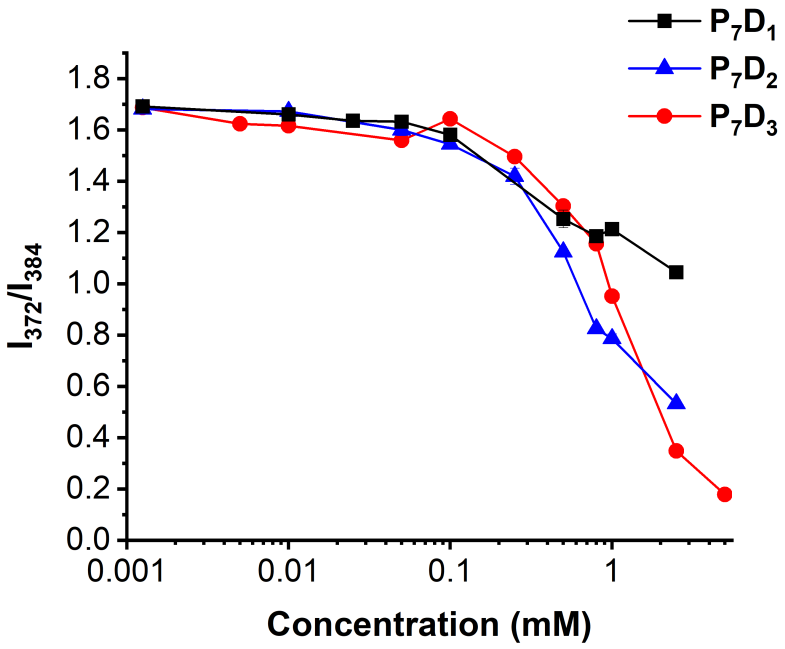

Fig. S10. Pyrene 1:3 ratios as a function of prodrug concentration

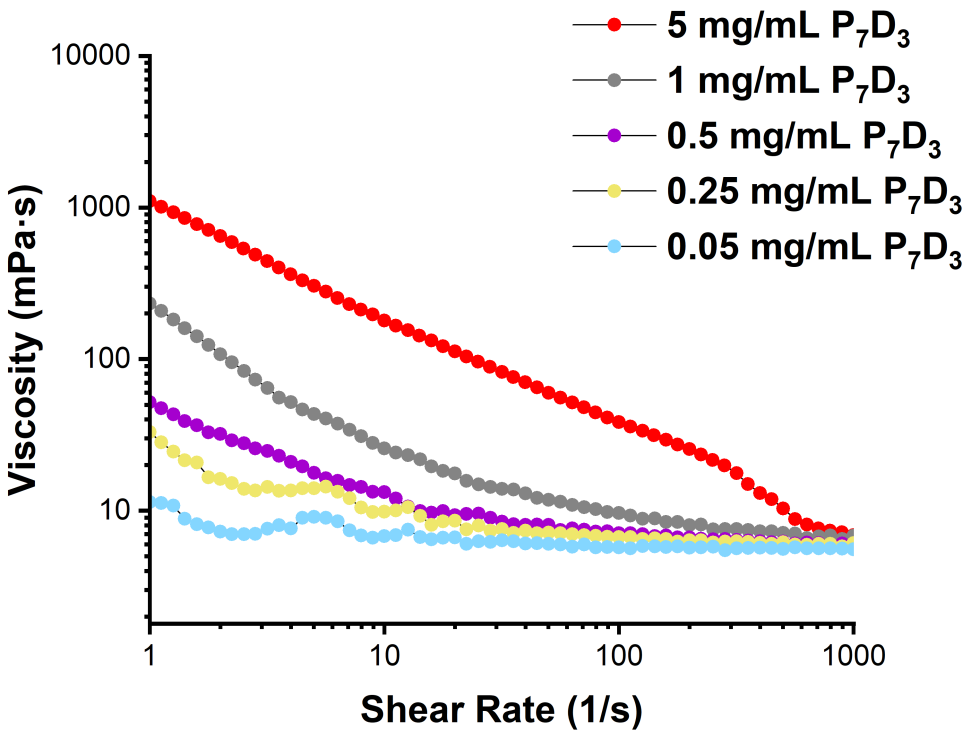

Fig. S11. Changes in viscosity and response to ramped shear rate for P7D3 solutions above and below their estimated CMC.

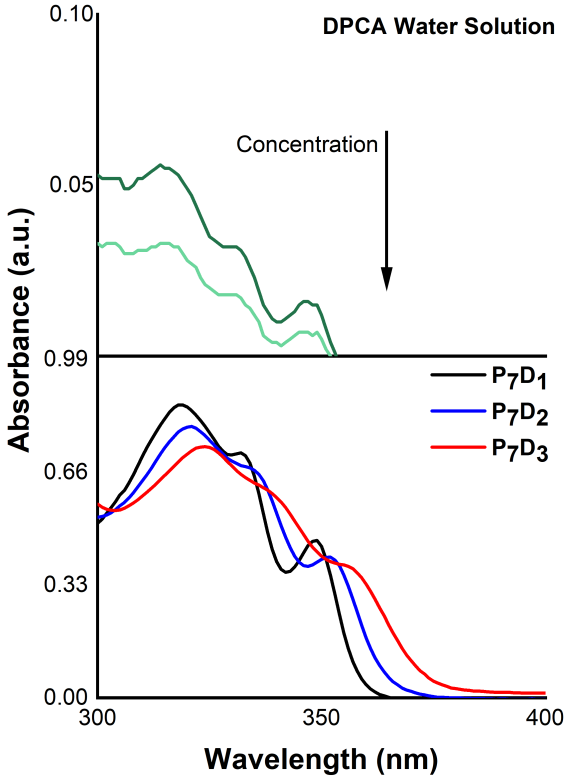

Fig. S12. UV-vis absorption spectra of aqueous solutions of DPCA (top) and PEG-DPCA prodrugs prepared at 0.1 mg/mL.

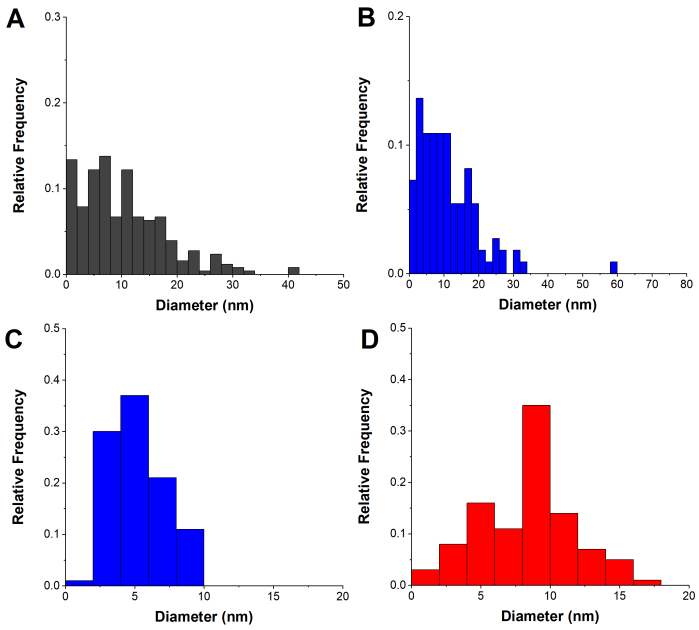

Fig. S13. Size distribution of P7D1 (A) and P7D2 (B) particles, and width of P7D2 (C) and P7D3 (D) fibers imaged in cryo-EM (n = 100 for all samples).

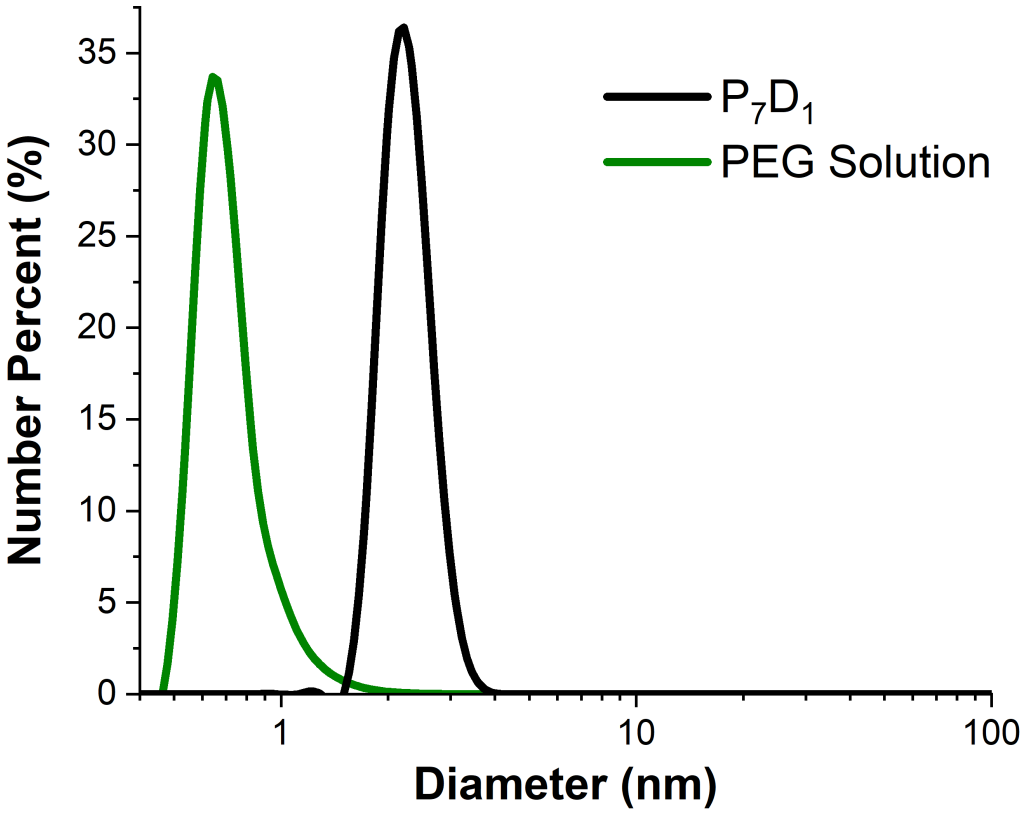

Fig. S14. Number distributions of 3 g/L P7D1 and PEG aqueous suspensions obtained via DLS.

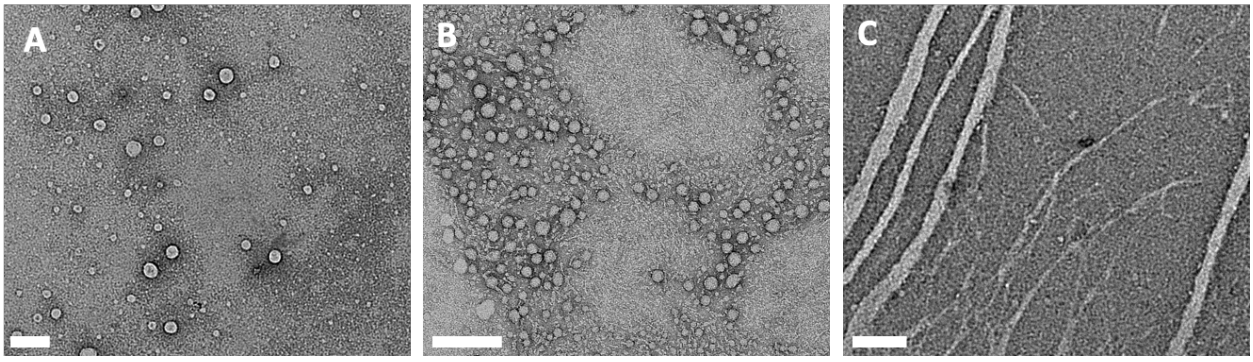

Fig. S15. TEM micrographs of PEG-DPCA prodrugs. Conventional, dry-state TEM was performed on 7 g/L aqueous dispersions for all samples. In corroboration with cryo-EM, spherical assemblies were observed for P7D1 (A) and P7D2 (B) samples, with the emergence of some worm-like micelles in P7D2 as well. For P7D3 (C), single fibers and bundles are observed. Scale bar = 200 nm

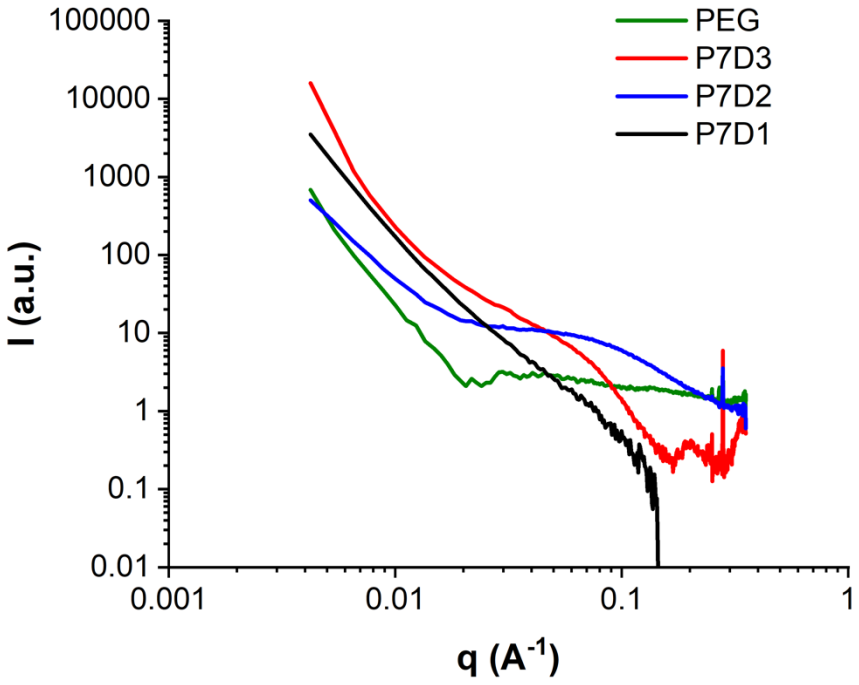

Fig. S16. 1D plot from SAXS analysis of P7D1, P7D2 and P7D3 and the reference PEG(750) solution, all in ultra-pure water.

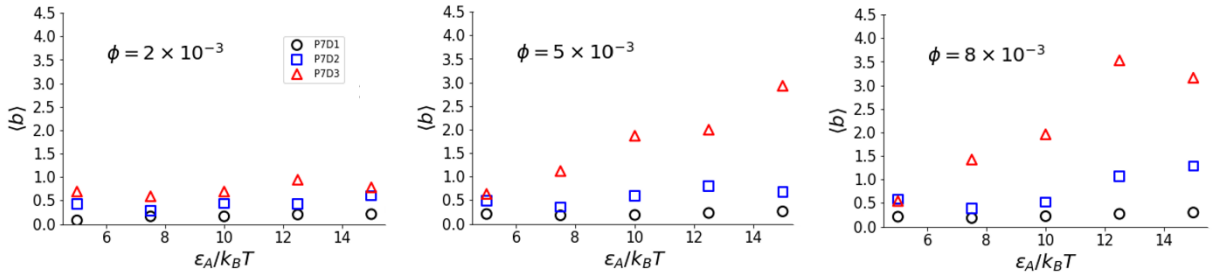

Fig. S17. Attraction strength dependence of average asphericity for ϕ = 0.002, 0.005, 0.008.

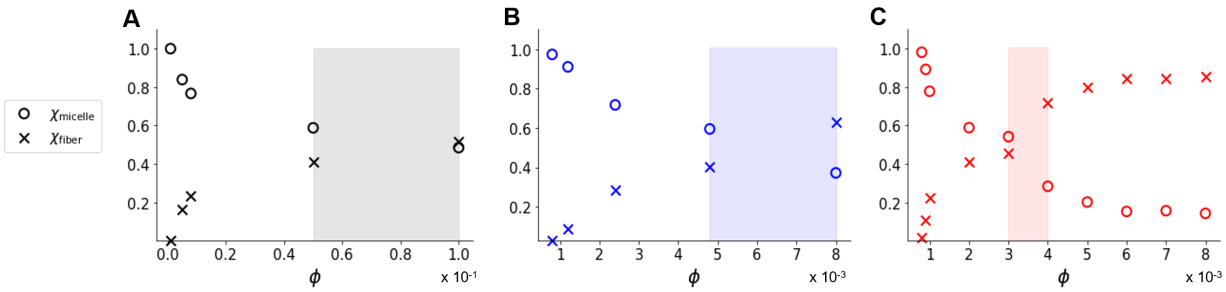

Fig. S18. Fraction of molecules in micelles $\chi_{micelle}$ and fibers χ_{fiber} at the same molecular attraction strength (i.e. P7D1 with ε_A = 30 k_BT, P7D2 with ε_A = 15 k_BT and P7D3 with ε_A = 10 k_BT). The shaded regions indicate the range of concentrations in which $\chi_{micelle}$ and χ_{fiber} must intersect, which would define the critical fiber concentration. The critical fiber concentration for P7D1 ($0.05 < \phi < 0.1$) is two orders of magnitude higher than that of P7D2 ($0.005 < \phi < 0.008$) and P7D3 ($0.003 < \phi < 0.004$).

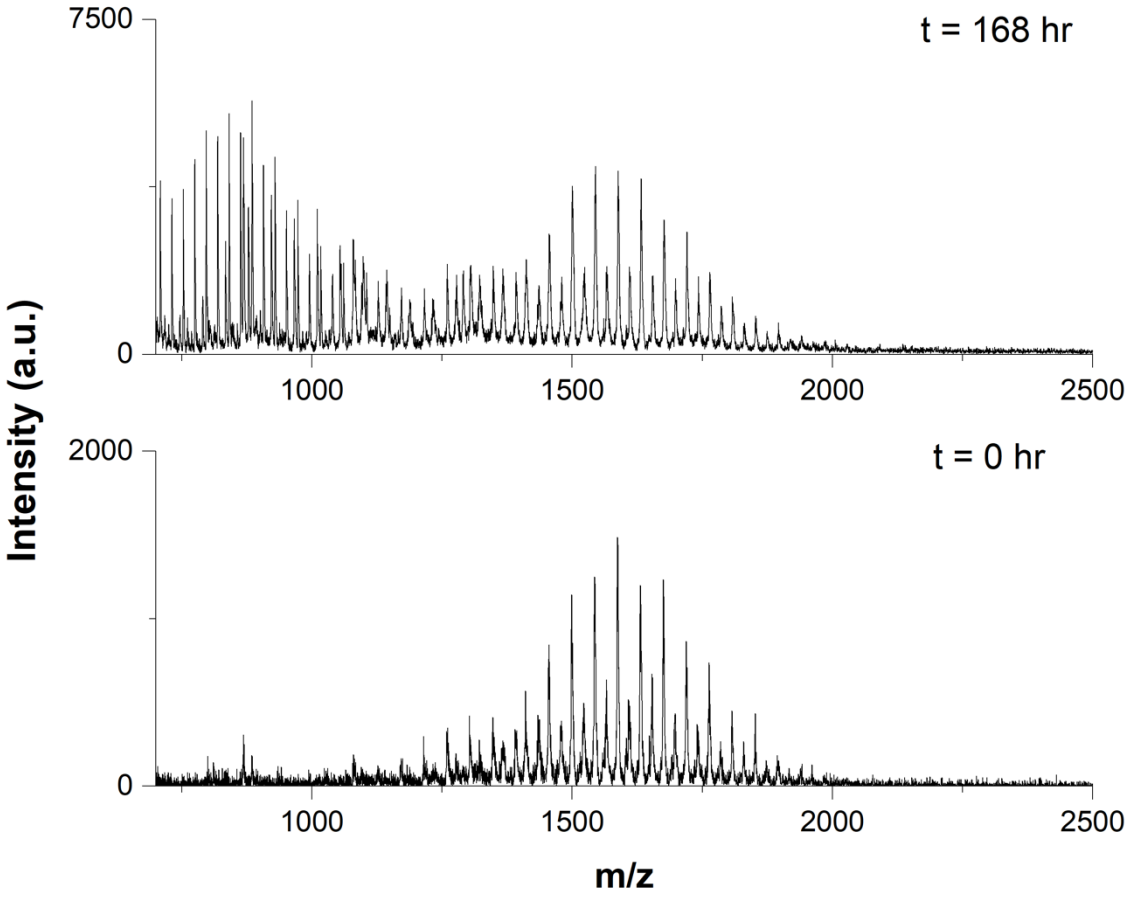

Fig. S19. MALDI-TOF-MS spectra of P7D3 samples before (t = 0hr) and during hydrolysis, highlighting the emergence of free and partially coupled PEG-DPCAs.

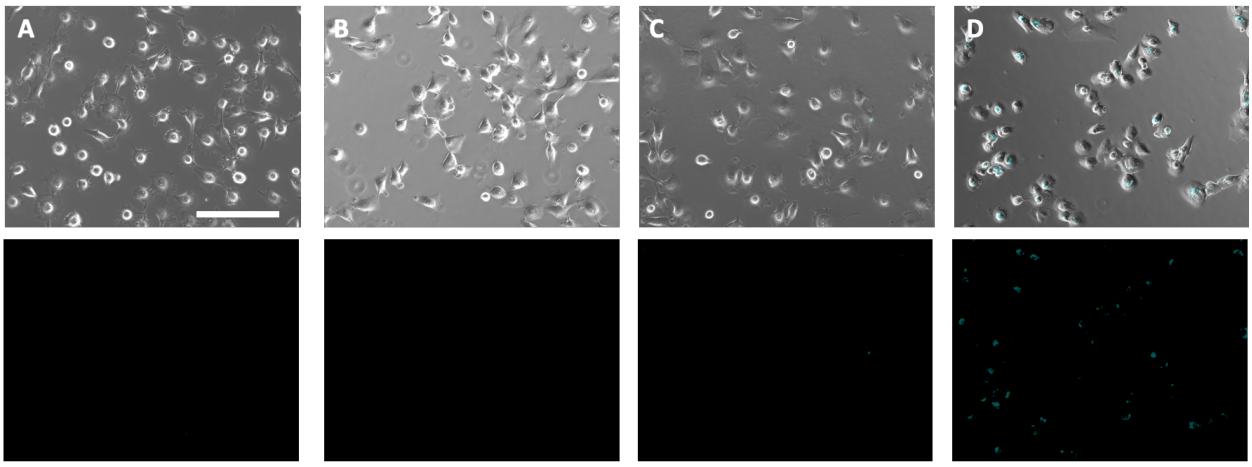

Fig. S20. Images of AECs treated with growth media (A), P7D1 (B), P7D2 (C), or P7D3 (D) for four hours. Prodrug concentrations were normalized to 0.2 mg/mL DPCA. DPCA fluorescence (bottom) was visualized at 405 nm excitation and overlayed with brightfield images (top). Scale bar = 200 um

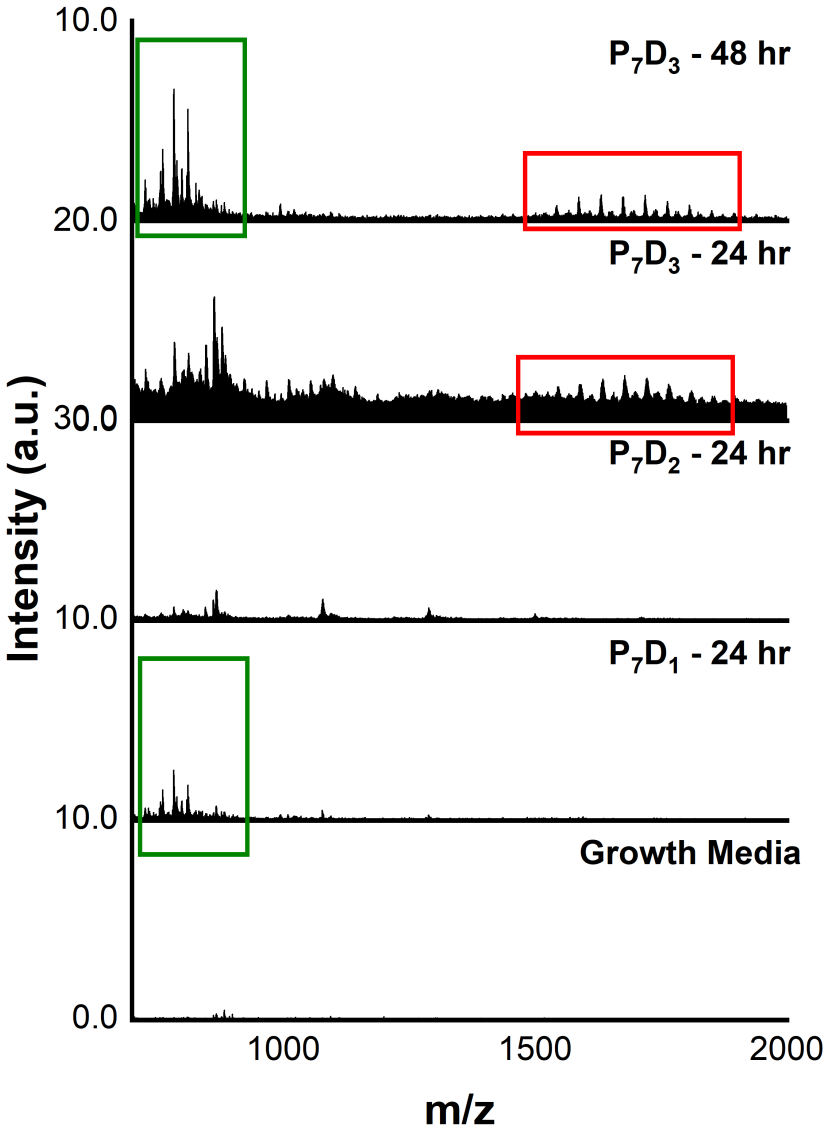

Fig. S21. MALDI-TOFMS of cellular lysates obtained from AECs incubated with growth media or PEG-DPCAs. Free PEG at 780 g/mol is highlighted by the green box. Evidence of P7D3 in lysates at 1680 g/mol is shown in red.

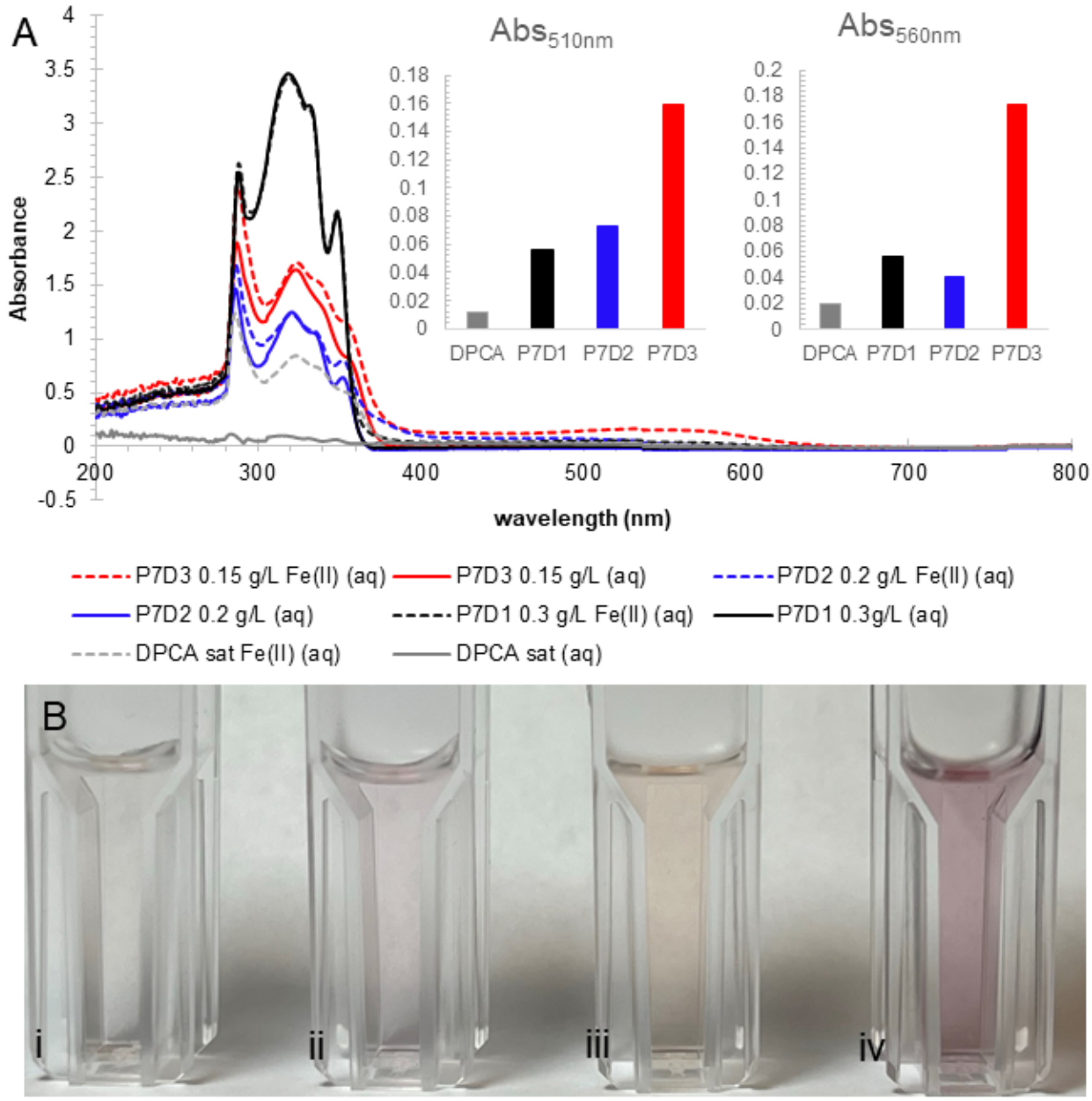

Fig. S22. UV-VIS absorbance analysis of solutions of DPCA and prodrugs (at 60µg/mL DPCA) before (solid lines) and after addition of $FeCl_2$ at 1:3 molar ratio Fe:DPCA waiting 1 hour (dashed lines); saturated DPCA solution (Grey), P7D1 (Black), P7D2 (Blue) and P7D3 (Red) (A). A photo of the cuvettes containing DPCA (i), P7D1 (ii), P7D2 (iii), and P7D3 (iv) after adding $FeCl_2$ and waiting 5 hours, emphasizing the difference in color (B). The inset in (A) shows the value of absorbance after subtracting the value before iron addition at that wavelength.

SI References

1. Y. Zhang, *et al.*, Drug-induced regeneration in adult mice. *Sci. Transl. Med.* **7**, 290ra92-290ra92 (2015).

2. J. Cheng, D. Amin, J. Latona, E. Heber-Katz, P. B. Messersmith, Supramolecular Polymer Hydrogels for Drug-Induced Tissue Regeneration. *ACS Nano* **13**, 5493–5501 (2019).

3. G. Ashiotis, *et al.*, The fast azimuthal integration Python library: {\it pyFAI}. *J. Appl. Crystallogr.* **48**, 510–519 (2015).

4. K. Kremer, G. S. Grest, Dynamics of entangled linear polymer melts: A molecular-dynamics simulation. *J. Chem. Phys.* **92**, 5057 (1998).

5. T. D. Nguyen, C. L. Phillips, J. A. Anderson, S. C. Glotzer, Rigid body constraints realized in massively-parallel molecular dynamics on graphics processing units. *Comput. Phys. Commun.* **182**, 2307–2313 (2011).

6. N. H. P. Nguyen, D. Klotsa, M. Engel, S. C. Glotzer, Emergent collective phenomena in a mixture of hard shapes through active rotation. *Phys. Rev. Lett.* **112**, 075701 (2014).